

The role of submillimetre galaxies in hierarchical galaxy formation.

Juan E. González^{1*}, C. G. Lacey¹, C. M. Baugh¹, C. S. Frenk¹

¹*Institute for Computational Cosmology, Department of Physics, Durham University, South Road, Durham DH1 3LE, UK*

ABSTRACT

We study the role of submillimetre galaxies (SMGs) in the galaxy formation process in the Λ Cold Dark Matter cosmology. We use the Baugh et al. semi-analytical model, which matches the observed SMG number counts and redshift distribution by assuming a top-heavy initial mass function (IMF) in bursts triggered by galaxy mergers. We build galaxy merger trees and follow the evolution and properties of SMGs and their descendants. Our primary sample of model SMGs consists of galaxies which had $850\mu\text{m}$ fluxes brighter than 5mJy at some redshift $z > 1$. Our model predicts that the present-day descendants of such SMGs cover a wide range of stellar masses $\sim 10^{10} - 10^{12} h^{-1} M_{\odot}$, with a median $\sim 10^{11} h^{-1} M_{\odot}$, and that more than 70% of these descendants are bulge-dominated. More than 50% of present day galaxies with stellar masses larger than $7 \times 10^{11} h^{-1} M_{\odot}$ are predicted to be descendants of such SMGs. We find that although SMGs make an important contribution to the total star formation rate at $z \sim 2$, the final stellar mass produced in the submillimetre phase contributes only 0.2% of the total present-day stellar mass, and 2% of the stellar mass of SMG descendants, in stark contrast to the popular picture in which the SMG phase marks the production of the bulk of the mass of present day massive ellipticals.

Key words: galaxies: evolution — galaxies: formation

1 INTRODUCTION

Our understanding of the star formation history of the Universe has changed dramatically as new populations of star-forming galaxies have been discovered at high redshifts. A key advance was the discovery of the cosmic far-infrared background by COBE (Puget et al. 1996), with an energy density similar to that in the UV/optical background, which implies that the bulk of star formation over the history of the Universe has been obscured by dust, with most of the radiation from young stars being reprocessed by dust grains to far-infrared and sub-mm wavelengths. This was followed by the discovery of the submillimetre galaxies (SMGs) using the Submillimetre Common User Bolometer Array (SCUBA) instrument on the James Clerk Maxwell Telescope (JCMT) (Smail et al. 1997; Hughes et al. 1998), which are generally interpreted as dust-enshrouded galaxies undergoing a starburst. Follow-up studies have concentrated on SMGs with $850\mu\text{m}$ fluxes brighter than about 5mJy . Spectroscopy has revealed that the bulk of such SMGs lie at redshifts $z \sim 1 - 3$, with a median around $z \sim 2$, when the Universe had only 20% of its current age (Chapman et al. 2005). Explaining the abundance and redshifts of SMGs has posed a challenge to theoretical models of galaxy formation ever since their discovery.

In the standard picture, due to the high star formation rates inferred in these galaxies (of $\sim 100 - 1000 M_{\odot} \text{yr}^{-1}$ for a standard initial mass function, e.g. Hughes et al. 1998; Chapman et al.

2004), the SCUBA phase is expected to play an important role in the build-up of the stars in massive galaxies. Central to this topic are the questions: do SMGs represent the assembly of massive present day ellipticals? What is the typical duration of the SCUBA phase? What are the typical stellar and host halo masses of their descendants? Do the descendants all have high masses, and are they preferentially spheroid-dominated? And finally, what is the overall contribution of the SCUBA phase to the stellar mass of present-day galaxies?

In this paper we address these questions using the predictions of a semi-analytical model for galaxy formation and evolution. A powerful feature of semi-analytical models is the ability to connect high redshift galaxies to their present-day descendants (Baugh 2006). Since it is believed that the dust plays a central role in producing the submillimetre radiation observed from SMGs, the model must take into account the energy reprocessed by dust when the spectral energy distribution (SED) is calculated.

The analysis in this paper is based on the Baugh et al. (2005) version of the GALFORM semi-analytical model. Baugh et al. found it necessary to assume a top-heavy initial mass function (IMF) for starbursts in order to reproduce the observed number counts and redshift distribution of the submillimetre galaxies, while also being consistent with other observational constraints, including the luminosity function of Lyman-break galaxies at $z \sim 3$, the present-day optical and near- and far-infrared luminosity functions, and the gas fractions and metallicities of present-day galaxies. In the Baugh et al. model, the SMGs seen in current surveys are mostly starbursts triggered by major and minor mergers between gas-rich

* E-mail: jegonzal@eso.org

disk galaxies. This model was subsequently shown to predict evolution of galaxies in the IR in good agreement with *Spitzer* observations (Lacey et al. 2008), and has also been used to make predictions for *Herschel* (Lacey et al. 2010c). The model also reproduces the local size-luminosity relation for late-type galaxies, and the fractions of early and late-type galaxies (González et al. 2009). González et al. (2010) perform a similar analysis to the one presented in this paper, but for Lyman-break galaxies, rather than SMGs. Lyman-break galaxies are identified using photometric selection to isolate the Lyman-break feature present in the rest-frame ultraviolet spectral energy distribution of star-forming galaxies (and which is accentuated due to absorption by gas along the line of sight to the galaxy). Lacey et al. (2010b) present a detailed study of the nature of Lyman-break galaxies in hierarchical galaxy formation models.

The semi-analytical galaxy formation approach has been used by other authors to model submillimetre galaxies. Kaviani et al. (2003) were able to reproduce the number counts of SCUBA sources, but only by treating the dust temperature as a free parameter, for which they needed to choose quite a low value (20–25 K), in apparent conflict with subsequent observations of sub-mm SED shapes (Coppin et al. 2008). Fontanot et al. (2007) reproduced the number counts of galaxies in the $850\mu\text{m}$ band using a self-consistent calculation of the dust temperature and a standard Salpeter initial mass function for all types of star formation, but their model does not match the observed redshift distribution of SMGs. Swinbank et al. (2008) tested the Baugh et al. (2005) model by comparing in detail the SEDs and stellar, dynamical, gas and halo masses of submillimetre galaxies against observational data, finding broad agreement. Recently Davé et al. (2010) have proposed an alternative model of SMGs based on hydrodynamical simulations, in which SMGs are massive galaxies undergoing quiescent star formation with a normal IMF. However, they do not calculate the sub-mm luminosities of their simulated galaxies, and so do not show that their model can reproduce the observed number counts and redshift distribution of SMGs. Prior to the present paper, no attempt has been made to relate the SMGs predicted in models with their present-day descendants.

This paper is laid out as follows. In Section 2, we outline the galaxy formation model GALFORM used to predict the properties of SMGs. In Section 3, we present examples from the model of galaxy evolution histories which produce SMGs. In Section 4, we study properties predicted for SMGs at different redshifts, such as stellar and host halo masses and morphologies, and also the duration of the SMG phase. In Section 5, we show the model predictions for the present-day descendants of SMGs, including their stellar and host halo masses and morphologies. In Section 6, we compute what fraction of present-day galaxies had SMG progenitors, and in Section 7 we calculate the contribution of SMGs to the present-day stellar mass density. Finally we present our conclusions in Section 8.

2 GALAXY FORMATION MODEL

2.1 Basic components

We use the Durham semi-analytical galaxy formation model, GALFORM, which is described in detail by Cole et al. (2000) and Benson et al. (2003). The model is set in the Cold Dark Matter (CDM) cosmology, with density parameter, $\Omega_0 = 0.3$, a cosmological constant, $\Omega_\Lambda = 0.7$, Hubble constant $H_0 = 70\text{km s}^{-1}\text{Mpc}^{-1}$,

baryon density, $\Omega_b = 0.04$ and a power spectrum normalization given by $\sigma_8 = 0.93$. Galaxies in the model are assumed to form inside dark matter haloes, and their subsequent evolution is controlled by the merging histories of the host dark matter haloes. The physical processes modelled include: i) the hierarchical assembly of dark matter haloes; ii) the shock heating and virialization of gas inside the gravitational potential wells of dark matter haloes; iii) the radiative cooling and collapse of the gas to form a galactic disk; iv) star formation in the cool gas; v) the heating and expulsion of cold gas through feedback processes such as stellar winds and supernovae; vi) chemical evolution of the gas and stars; vii) mergers between galaxies within a common dark halo as a result of dynamical friction; viii) the evolution of the stellar populations using population synthesis models; ix) the extinction and reprocessing of starlight by dust.

The merger histories of dark matter haloes are calculated using a Monte Carlo technique, following the formalism of extended Press & Schechter theory (Press & Schechter 1974; Lacey & Cole 1993; Cole et al. 2000). The formation and evolution of a representative sample of dark matter haloes is modelled.

We use the same galaxy formation parameters adopted by Baugh et al. (2005), but we use a modified version of the Monte Carlo merger trees (Parkinson et al. 2008), which better reproduces the properties of dark matter halo merger trees extracted from the Millennium Simulation (Springel et al. 2005). This is necessary because we wish to connect high redshift galaxies with their present-day descendants, and so we need a prescription for building merger histories of dark matter haloes which is accurate over a long interval in time. The Parkinson et al. algorithm for building halo merger trees is a modified version of that introduced by Cole et al. (2000) and used in Baugh et al. (2005), and has been tuned to match the merger histories extracted from the Millennium Simulation. This modification does not significantly affect the published predictions of the Baugh et al. model, since those did not depend on the accuracy of the trees over long time intervals. Instead, Baugh et al. laid down grids of halos at a range of redshifts to compute the number counts of SMGs and the cosmic star formation history. We have checked that using the Parkinson et al. tree algorithm does not alter the predictions presented in Baugh et al.

The Baugh et al. (2005) model uses feedback from a superwind to suppress the formation of massive galaxies and uses a top-heavy stellar IMF in starbursts triggered by galaxy mergers to reproduce the observed numbers of submillimetre and Lyman-break galaxies. An alternative model was presented by Bower et al. (2006), which adopts a standard IMF throughout, but uses AGN feedback to reduce the number of massive galaxies. However, the Bower et al. model underpredicts the number counts of submillimetre by more than an order of magnitude, so we do not consider it further here. For a complete list of the differences between these two models, see González et al. (2009).

2.2 Mergers and star formation bursts

When dark matter haloes merge, the galaxy in the most massive halo is assumed to become the central galaxy in the new halo while the other galaxies become satellites (note that the central galaxy identified in this way is not necessarily the most massive galaxy in the new halo). The model assumes that both central and satellite galaxies can form stars from their cold gas reservoirs, but only central galaxies can accrete more cold gas by cooling from the surrounding halo. (Font et al. (2008) considered an alternative model in which the hot gas halos of satellite galaxies are only partly

stripped, but this has little effect on SMGs in our model, which are typically central galaxies.)

Mergers in the model are assumed to happen only between satellite and central galaxies within the same halo. Bursts of star formation in the model are triggered by galaxy mergers. Two types of mergers are defined, major mergers and minor mergers, according to whether or not the ratio of the mass of the smaller galaxy to the larger galaxy M_2/M_1 exceeds the threshold f_{ellip} . Bursts are assumed to be triggered in all major mergers, but also in minor mergers that satisfy $M_2/M_1 > f_{\text{burst}}$ and where the ratio of gas to stellar plus gas mass of the larger galaxy exceeds $f_{\text{gas,crit}}$. The values adopted in the Baugh et al. model are $f_{\text{ellip}} = 0.3$, $f_{\text{burst}} = 0.05$ and $f_{\text{gas,crit}} = 0.75$. Mergers can change the morphologies of galaxies. In a major merger, the stellar disks of the merging galaxies are assumed to be transformed into a new stellar spheroid (resulting in a pure bulge galaxy) and any gas present in the disks is converted into stars in the burst, or ejected by supernova feedback associated with the burst. In minor mergers, the stellar disk of the larger galaxy is preserved and the stars from the smaller galaxy are added to its bulge, so the merger remnant is a disk+bulge galaxy. If the condition for a burst in this minor merger is satisfied, then the gas of the smaller galaxy is converted into stars and added to the bulge, while if the condition is not satisfied, any gas is added to the main gas disk.

As shown in Baugh et al. (2005), our model predicts that most SMGs seen in current sub-mm surveys are starbursts triggered by major and minor mergers involving gas-rich disk galaxies. Dekel et al. (2009, and references therein) have proposed a picture in which the most actively star forming galaxies at high redshifts are fed by cold streams of gas falling into galaxy halos. Although this picture appears very different from our model, the differences are actually less dramatic than they appear at first sight. Firstly, the GALFORM semi-analytical model has always included a “cold” mode of accretion, in which gas falls to the halo centre at the free-fall rate, for halos in which the cooling time is less than the free-fall time for gas shocked at the virial radius (Cole et al. 2000). This “cold” mode dominates at lower halo masses and higher redshifts. Benson & Bower (2010) have recently shown that using the Birnboim & Dekel (2003) criterion to distinguish “cold” and “hot” accretion modes instead of the standard GALFORM criterion slightly shifts the halo mass at which the transition from “cold” to “hot” accretion occurs, but leaves gas accretion rates and SFRs in the model almost unchanged. They also find that the importance of the “cold” mode is greatly reduced when realistic feedback is included. Secondly, in the Dekel et al. picture, the bright SMGs are actually triggered by the infall of large clumps of cold gas rather than smooth streams – effectively gas-rich galaxy mergers.

2.3 Top-heavy IMF in bursts

As mentioned in the introduction, an important feature of the Baugh et al. model is that stars are assumed to form with different initial mass functions (IMFs) in different environments. This differentiation depends on whether they form quiescently in disks or in bursts following a galaxy merger. In the case of disks, the model adopts a standard solar neighbourhood IMF proposed by Kennicutt (1983), for which the number of stars produced varies with mass as $dN/d\ln m \propto m^{-x}$, with $x = 0.4$ for $m < 1M_{\odot}$ and $x = 1.5$ for $m > 1M_{\odot}$. In the case of bursts, a top-heavy IMF is used, where $x = 0$. In either case, the IMF covers a mass range $0.15 < m < 120M_{\odot}$. This top-heavy IMF in bursts has two effects in the model: i) it increases the total UV radiation from the

young stars formed and ii) it increases the metal production and hence also the amount of dust.

When stars die, they return gas and metals to the interstellar medium (ISM). We treat this process using the instantaneous recycling approximation, in which the metal ejection is quantified by the yield, p , (which is the mass of metals returned to the ISM per unit mass of stars formed) and the gas return is specified by the recycled fraction, R , (defined as the mass of gas returned to the ISM per unit mass of stars formed). We have calculated the values of p and R for our two IMFs based on the results of stellar evolution calculations (Cole et al. 2000; Baugh et al. 2005), and find values $p_{\text{quiescent}} = 0.023$, $R_{\text{quiescent}} = 0.41$ for quiescent star formation and $p_{\text{burst}} = 0.15$, $R_{\text{burst}} = 0.91$ for bursts.

There is independent support for the idea of variations in the IMF from a variety of observations, as discussed in Lacey et al. (2008). We mention a few of these here. Fardal et al. (2007) found a discrepancy between the observed ratio of the total extragalactic background radiation to the observed stellar density today and the value predicted using the observationally inferred star formation history, if a standard IMF is assumed. They find that a more top-heavy IMF is needed (increasing the proportion of stars formed with $1.5M_{\odot} < m < 4M_{\odot}$) in order to reconcile these different observations. They argue that alternative solutions in which non-stellar sources make large contributions to the background light appear unlikely to resolve the discrepancy. Another suggestion of variations in the IMF comes from the work of van Dokkum (2008), who compares the luminosity evolution of massive cluster galaxies (at $0.02 \leq z \leq 0.83$) with their colour evolution. He finds that the evolution of the rest-frame $U - V$ colour is not consistent with the previously determined evolution of the rest-frame M/L_B ratio for a standard IMF, but shows that using a different IMF with a flatter slope compared with a standard IMF can help to solve the discrepancy.

2.4 Reprocessing of stellar radiation by dust

The IR/sub-mm emission detected from SMGs is believed to originate from the dust heated by radiation from young stars. Therefore a treatment of absorption and reemission of radiation by dust is a key element of the model. In Baugh et al. (2005), we calculated the reprocessing of stellar radiation by dust using the GRASIL code (Silva et al. 1998; Granato et al. 2000), which calculates the distribution of dust grain temperatures within each galaxy based on a radiative transfer calculation and a detailed grain model. The GRASIL model has been shown to be able to very successfully explain the SEDs of spiral, irregular, elliptical and starburst galaxies, including ULIRGS, over a huge range of wavelength, from the far-UV to the radio (Silva et al. 1998; Vega et al. 2008; Schurer et al. 2009). However, a drawback of the GRASIL code is that it takes several minutes of CPU to run a single galaxy, and so it is very time-consuming to run it on large samples of galaxies. For the present paper, we need to follow the evolution (including the sub-mm emission) of large samples of galaxies over many timesteps, in order to be able to select the small fraction of galaxies undergoing an SMG phase at any cosmic time, and it is not computationally feasible to do this using the GRASIL code directly.

We have therefore developed a simplified model of dust emission which approximately reproduces the results from the GRASIL code at long wavelengths. At the sub-mm wavelengths of interest here, the SED of dust emission is insensitive to details of the dust model such as the dust grain size distribution and the effects of small grains and PAH molecules, allowing us to apply a simpler

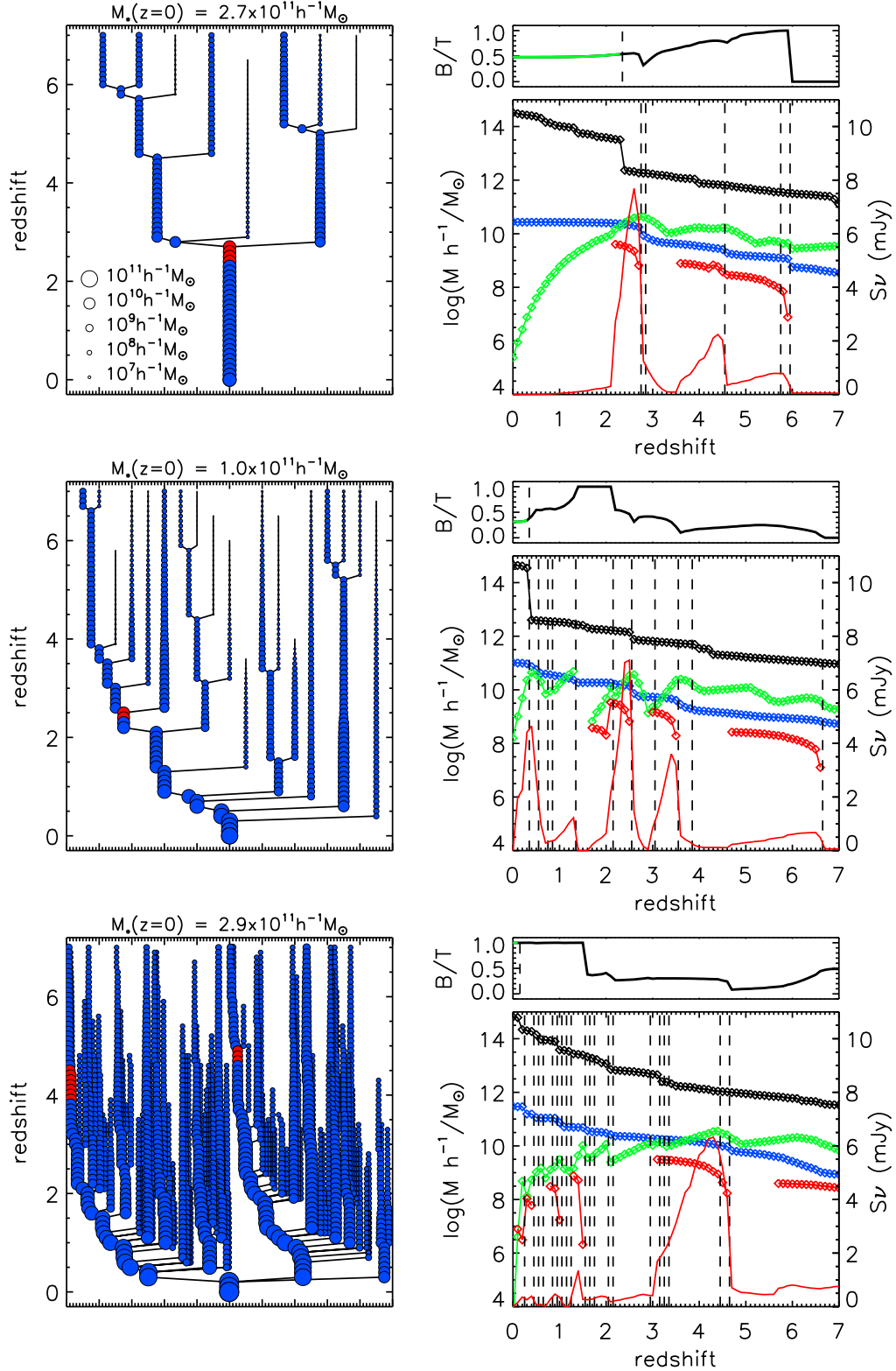


Figure 1. Left panels: galaxy merger trees for different $z = 0$ galaxies. The size of the symbol is proportional to the stellar mass as indicated by the key. The red circles indicate galaxies in a bright SMG phase (when the $850\mu\text{m}$ flux exceeds 5 mJy). Right panels: evolution with redshift of the galaxy on the main progenitor branch. Top subpanels: evolution of the bulge-to-total stellar mass ratio (B/T). The dashed vertical line indicates the redshift at which the central galaxy (black line) becomes a satellite galaxy (magenta line) after a halo merger. Lower subpanels: the symbols show the evolution of the stellar mass (blue), cold gas mass (green), dark matter host halo mass (black) and the mass formed in ongoing bursts (red) in units shown on the left axis. The red line shows the evolution of the $850\mu\text{m}$ flux, in units shown on the right axis, and the dashed vertical black lines indicate the redshift at which the galaxy undergoes a merger with another galaxy (see left panel). From top to bottom, the stellar masses of the galaxies at $z = 0$ are $M_* = 2.7 \times 10^{10}, 1.0 \times 10^{11}, 2.9 \times 10^{11} h^{-1} M_\odot$ respectively. In the case of the upper two galaxy trees, we show all of the progenitors with stellar mass in excess of $10^6 h^{-1} M_\odot$; in the lower tree, we plot progenitors with stellar mass greater than $10^8 h^{-1} M_\odot$.

approach. As in GRASIL, we assume that the dust is in two phases, molecular clouds and a diffuse medium, with stars forming inside the molecular clouds and then escaping into the diffuse medium on a timescale of a few Myr. We use an approximate radiative transfer calculation (different from the one in GRASIL itself) to compute how much stellar radiation is absorbed in each dust component. The most important difference with GRASIL is that in our simplified model we assume the dust temperature within each of the dust phases is uniform (so there are only two dust temperatures in a galaxy). In contrast, in GRASIL each size and composition of dust grain has its own temperature, which depends on position within the galaxy (which determines the intensity of the stellar radiation field which heats it, via the radiative transfer calculation). Furthermore, GRASIL includes the effect of fluctuating grain temperatures for small grains and PAH molecules. Thus in a full GRASIL calculation, there is a whole distribution of dust temperatures within each galaxy. A final approximation we make in our simplified dust model is to represent the dust emissivity by a power law in wavelength. These differences between our two-temperature model and GRASIL are crucial when calculating the dust emission at mid-IR wavelengths (which is dominated by emission from small grains and PAH molecules, and by warm dust in star-forming clouds), but have much less effect at the sub-mm wavelengths of interest in this paper. We give more details about our simplified dust model in Lacey et al. (2010a), where we also show some comparisons with GRASIL. In summary this model works remarkably well at long wavelengths in the Rayleigh-Jeans tail of the modified black body spectrum of the dust emission.

3 GALAXY MERGER TREES: EXAMPLES WITH SMG PROGENITORS

To follow galaxy evolution in GALFORM we output the model predictions at different redshifts. We label a galaxy as a bright SMG when its $850\mu\text{m}$ flux exceeds 5 mJy. As examples of different merger histories which can produce bright SMGs, we plot in the left panels of Fig. 1, galaxy merger trees for three different present-day galaxies, covering a range in present stellar mass from $\sim 3 \times 10^{10} h^{-1} M_{\odot}$ to $\sim 3 \times 10^{11} h^{-1} M_{\odot}$. In these examples we require that a SMG phase appears in the main progenitor branch (leftmost branch), which we define as follows: starting at the final time, we step back in time (up the tree), following the branch of the progenitor with larger stellar mass each time there is a merger. (Note that the main progenitor need not be the most massive progenitor at all times.) We indicate with a red circle when a galaxy at a given redshift is a bright SMG and with a blue circle otherwise. In these selected examples, the more massive present-day galaxies can show more than one bright SMG episode.

In the right panels of Fig. 1 we show the evolution of the $850\mu\text{m}$ flux for the main progenitor galaxy (leftmost branch) in the trees. Following each merger that triggers a burst, there is a rapid increase in the $850\mu\text{m}$ flux, followed by a slow decline. The time interval when the flux is above 5 mJy is different in the different examples. In the same panels, we also plot the evolution of the stellar, gas and dark matter halo masses for the main progenitor, together with the mass formed in ongoing bursts. In the upper sub-panels, we plot the evolution of the bulge-to-total stellar mass ratio B/T as an indication of the morphology of the galaxy, and we also indicate when the central galaxy became a satellite galaxy.

In the first example shown in Fig. 1, the central galaxy becomes a satellite galaxy at $z = 2.3$ (note the large increase in the

host halo mass due to the merger with a more massive halo). In the second example, the galaxy becomes a satellite at $z = 0.3$ and in the third example, the galaxy becomes a satellite at $z = 0.1$. As mentioned previously, in the standard GALFORM scheme, satellite galaxies cannot accrete any more gas by cooling, so star formation can only continue until the pre-existing cold gas reservoir is used up, which limits the increase in stellar mass once a galaxy becomes a satellite (green line).

We also indicate in the right-hand panels when the galaxy undergoes a merger with another galaxy. If there is a burst (see Section 2.3) the gas from the merging pair is used up to produce a burst of star formation (which raises the $850\mu\text{m}$ flux). Note that the galaxy mergers at $z = 2.7$ and $z = 2.5$ in the first and second examples, respectively, are minor mergers since the morphology of the resulting galaxy is a mix of bulge+disk ($B/T \sim 0.5$ in both cases). The galaxy mergers at $z = 5.9$ and $z = 2.1$ in the first and second examples, respectively, are major mergers since the resulting galaxy is a pure bulge galaxy with $B/T = 1$. Since more hot gas can be accreted by cooling onto central galaxies, more star formation takes place, changing again the morphology of the galaxy. In the third example, the main progenitor becomes bulge dominated following a major merger at $z \sim 1.5$ and remains bulge dominated, even though it is still the central galaxy in its halo until $z = 0.1$. In this example, there are a number of mergers with other galaxies which add mass to the spheroid (indicated by the vertical dashed lines in the main panel on the bottom right).

4 PROPERTIES OF SMGS AT DIFFERENT REDSHIFTS

Having identified all the SMGs in the model, we can study the evolution of their properties. In the model, the redshift distribution of SMGs shows a peak at $z \sim 2$ (Baugh et al., see also Swinbank et al.) similar to that observed by Chapman et al. (2003, 2005). For convenience in what follows, we define two types of submillimetre galaxies according to a threshold in the $850\mu\text{m}$ flux. We define a galaxy as a *bright* SMG when its flux exceeds 5 mJy and as a *faint* SMG when its flux exceeds 1 mJy. The faint sample therefore includes the bright sample, but these bright galaxies only account for a small fraction of the galaxies in the faint sample. Most currently observed SMGs have fluxes around 5 mJy or brighter (and so are bright SMGs by the definition used here). We present the faint SMGs as a comparison sample.

Our samples of SMGs are effectively volume limited. We consider dark matter halo merger histories for a grid of halo masses, generating many different examples for each mass on the grid. SMGs are identified according to their flux as outlined above, given the redshift of a particular branch in the merger history. The distributions of properties from different mass trees are combined by assigning a weight to each tree based on the abundance of haloes of that mass and the number of example histories produced.

4.1 Duration of the SMG phase

We define the duration of the bright SMG phase to be the time for which the $850\mu\text{m}$ flux of a galaxy is above 5 mJy. This time is typically smaller than the duration of the star formation burst which triggered the flux increase (see the examples in Fig. 1). In Fig. 2 we plot the distribution of SMG phase durations all of the bright SMG phases identified in the redshift range $2 < z < 3$. The distribution is that for a volume-limited sample. The durations range from < 0.04 Gyr to roughly 0.5 Gyr. The median of the

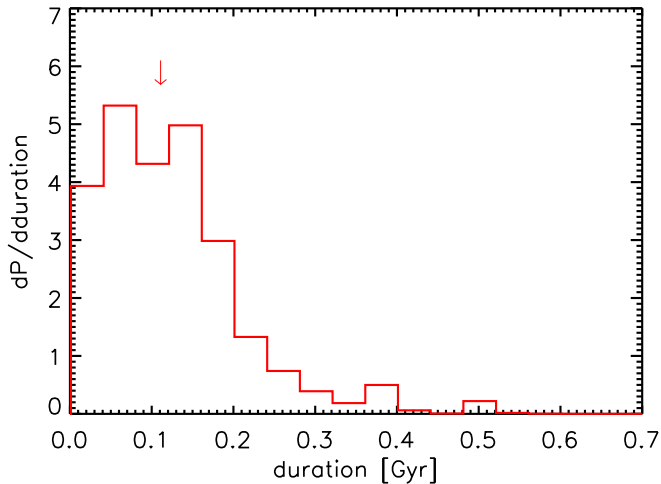


Figure 2. Duration of the bright SMG phase, i.e. the time for which the flux is $S_\nu(850\mu m) > 5\text{mJy}$, for SMGs at $2 < z < 3$. The distribution is that for a volume-limited sample. The median of the distribution is 0.11 Gyr (indicated by the arrow). The distribution is normalized to unit area.

distribution is 0.11 Gyr. For comparison, the median duration of the star formation bursts that triggered the bright SMG phase is 0.66 Gyr. These predicted durations are similar to observational estimates based on UV spectral fitting (Smail et al. 2003), duty cycle arguments (Chapman et al. 2005) and gas depletion timescales (Tacconi et al. 2006).

4.2 Stellar and Halo Masses

The left-hand panels of Fig. 3 show the median stellar and halo masses of SMGs identified at different redshifts (the right-hand panels of this plot show the properties of the descendant galaxies and are discussed in the next section). The medians are calculated for volume-limited samples of SMGs at each redshift. The top left panel of Fig. 3 shows the median stellar mass and host halo mass for the bright SMGs as a function of redshift. For the bright SMG sample at redshift $z=1.5$, the stellar and parent halo mass are respectively 4 and 2 times more massive than the bright SMGs identified at redshift $z=6$. For comparison, we show also the results for faint SMGs (i.e. those with $S_\nu > 1\text{mJy}$) in the bottom left panel. Faint SMGs identified at redshift $z=6$ have typically 1/4 of the stellar mass of the bright SMGs identified at the same redshift, and they live in haloes with 1/3 the mass. By redshift $z=1.5$, this difference in host masses of faint relative to bright SMGs has shrunk to around a factor 0.7 for both stellar and halo masses.

At redshift $z = 2$, close to the median redshift of bright ($S_\nu > 5\text{mJy}$) SMGs (both in the model and in the observational data), the model predicts median stellar masses of 2.1×10^{10} and $1.7 \times 10^{10} h^{-1} M_\odot$ for the bright and faint SMGs, and host halo masses of 2.2×10^{12} and $1.5 \times 10^{12} h^{-1} M_\odot$ respectively. The predicted stellar and halo masses of SMGs in this model were compared with observational constraints in Swinbank et al. (2008). The main observational constraint on halo masses comes from measurements of galaxy clustering. Swinbank et al. found good agreement between preliminary predictions of SMG clustering from the model and observational data, but this issue will be examined in more detail in Almeida et al. (2010). Swinbank et al. also found that the predicted stellar masses of SMGs were lower than observational estimates based on fitting stellar population models to

broad-band fluxes. However, this comparison is complicated by the fact that the model includes a top-heavy IMF in starbursts, while the observational estimates assume a solar neighbourhood IMF for all stars (see also the discussion in Lacey et al. (2010b)). A more recent observational analysis by Hainline et al. (2010), using updated stellar population models and correcting for AGN contamination of the rest-frame near-IR light, finds a median stellar mass of $\sim 5 \times 10^{10} h^{-1} M_\odot$, for a sample of SMGs with $S_\nu \sim 5\text{mJy}$ and $z \sim 2$, assuming a Kroupa (2001) IMF. (Note that the typical stellar masses found by Hainline et al. are significantly lower than the values estimated by Michałowski et al. (2010) for a similar SMG sample, but not allowing for AGN contamination of the broad-band SED.) The median stellar mass found by Hainline et al. is not very different from the median value predicted by our model for bright SMGs at $z = 2$, even before allowing for the difference in IMFs and star formation histories between the model and what is assumed in the observational analyses. We will investigate this issue in more detail in a future paper.

4.3 Morphology

In a similar way, we can study the morphologies of SMGs identified at different redshifts. As mentioned above, a major merger produces a pure bulge galaxy, whereas a minor merger can result in a galaxy with a disk and a bulge (if the primary galaxy had a disk at the moment of merging). Note that in our model, the starburst responsible for a galaxy appearing as an SMG starts *after* the two galaxies have merged. The left-hand panels of Fig. 4 show the model predictions for the B/T ratio of SMGs identified at different redshifts, and the right-hand panels, which we discuss in the next section, show B/T for SMG descendants. As in Fig. 3, the medians are calculated for volume-limited samples of SMGs at each redshift. In the top left panel of Fig. 4, we plot the median of the bulge-to-total stellar mass ratio B/T (where $B/T=0$ indicates a pure disk galaxy and $B/T=1$ indicates a pure bulge galaxy) for the bright SMGs. At high redshift, bright SMGs have intermediate values of B/T ($B/T \sim 0.4$), but the typical B/T increases to ~ 0.7 (indicating a bulge-dominated galaxy) as the redshift decreases to $z \sim 1$, before dropping again to $B/T \sim 0.4$ at lower redshifts. At $z = 2$, bright SMGs are predicted to have a median $B/T = 0.6$, indicating a mildly bulge-dominated galaxy, but with quite a broad distribution, from 0.4 to 1 (10-90% range).

For comparison, we show also the results for faint SMGs selected with $S_\nu > 1\text{mJy}$ in the bottom left panel of Fig. 4. These faint SMGs typically have intermediate values of B/T at all redshifts, with a very wide range (from 0.1 to 1), and the samples at higher redshifts have slightly higher values of B/T compared to those at lower redshift (showing an opposite trend as compared to bright SMGs).

Swinbank et al. (2010) have recently investigated the morphologies of bright SMGs at $z \sim 2$ using HST optical and near-IR imaging. They find that the light profiles are fit by Sérsic indices $n \sim 2 - 2.5$, compared to the values $n = 1$ and $n = 4$ expected for exponential disks or $r^{1/4}$ -law spheroids respectively. This result indicates that these SMGs are mildly bulge-dominated, entirely consistent with the B/T values predicted by our model for SMGs at similar fluxes and redshifts.

4.4 The SMG phase trigger: minor or major mergers?

As we discussed before, most ($> 99\%$) of bright SMGs in our model are starbursts triggered by galaxy mergers. Bursts happen

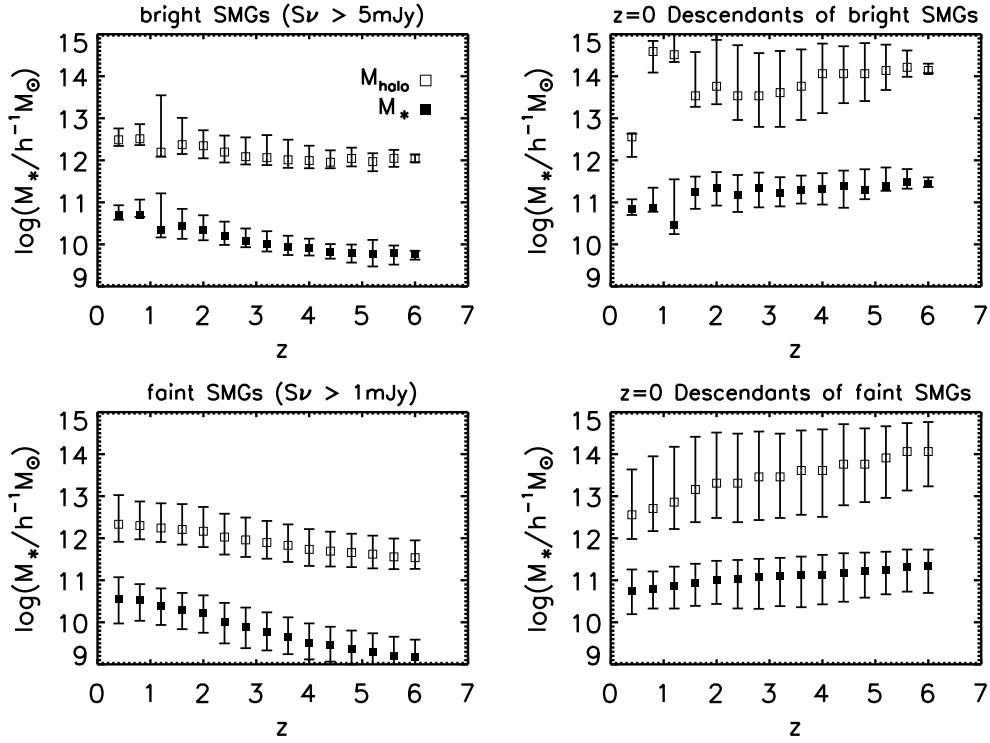


Figure 3. Left panels: The median stellar and host halo masses for SMGs selected at different redshifts. Right panels: median stellar and host halo masses of the $z=0$ descendants of SMGs identified at different redshifts. Top panels: bright SMGs selected with $S_\nu > 5\text{mJy}$. Bottom panels: faint SMGs selected with $S_\nu > 1\text{mJy}$. Filled squares show stellar masses and open squares show halo masses. Errorbars indicate the 10% and 90% percentiles. The medians are all calculated for volume-limited samples of SMGs at each redshift.

in all major mergers and in some minor mergers (see Section 2.3). Which type of merger dominates the triggering of SMGs? We answer this question in Fig. 5, where we plot the distribution of stellar masses of $z = 0$ descendants of bright SMGs at $z > 1$ separated into those triggered by minor mergers (blue) and produced by major mergers (red). In this plot, we have weighted the contributions to the distribution from the different redshift intervals by the co-moving volume per solid angle, so that the final distribution (which is normalized to unit area under the histogram) corresponds to what would be seen in a flux-limited sample of SMGs over a fixed solid angle. We find that 77% are produced by minor mergers, 22% are produced by major mergers, and 0.7% are quiescent galaxies (i.e. not ongoing starbursts). Minor and major mergers are responsible for similar numbers of SMGs for the highest descendant masses, but for all other descendant masses, minor mergers predominate. These proportions are qualitatively consistent with the result shown in Fig. 4 that the bulge-to-total stellar mass ratios B/T of SMGs are typically intermediate between pure disk and pure bulge.

5 PROPERTIES OF SMG DESCENDANTS

Most of the SMGs detected in flux-limited surveys lie at redshifts $z=1-4$. SMGs at redshift $z < 1$ account for only a small fraction of the population in a flux limited sample due to the relatively small volume at low redshift. Model SMGs at low redshifts $z < 1$ are mostly objects with modest star formation rates which have bright sub-mm fluxes simply due to their proximity to us compared with the bulk of the SMG population, rather than because an intense episode of star formation has taken place. In this section, we will

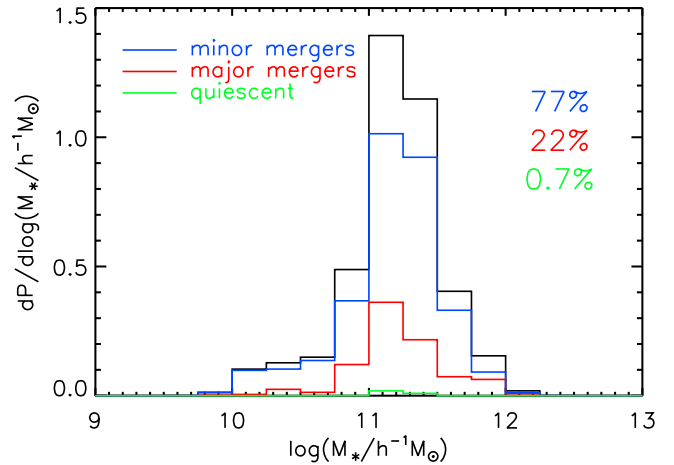


Figure 5. The distribution of stellar masses of the descendants of bright ($S_\nu > 5\text{mJy}$) SMGs at $z > 1$, showing the separate contributions of SMGs produced by major mergers (red), minor mergers (blue) and quiescent galaxies (green). The contributions to this distribution from different redshifts have been weighted so as to correspond to what would be seen in a flux-limited survey over a fixed solid angle. The total distribution is normalized to have unit area.

focus on the descendants of the *high- z* SMGs, which we define to be those with $z > 1$ on the basis that these have the largest overlap with observational samples, and we will investigate the distribution in stellar and parent halo mass, morphology and central/satellite galaxy classification.

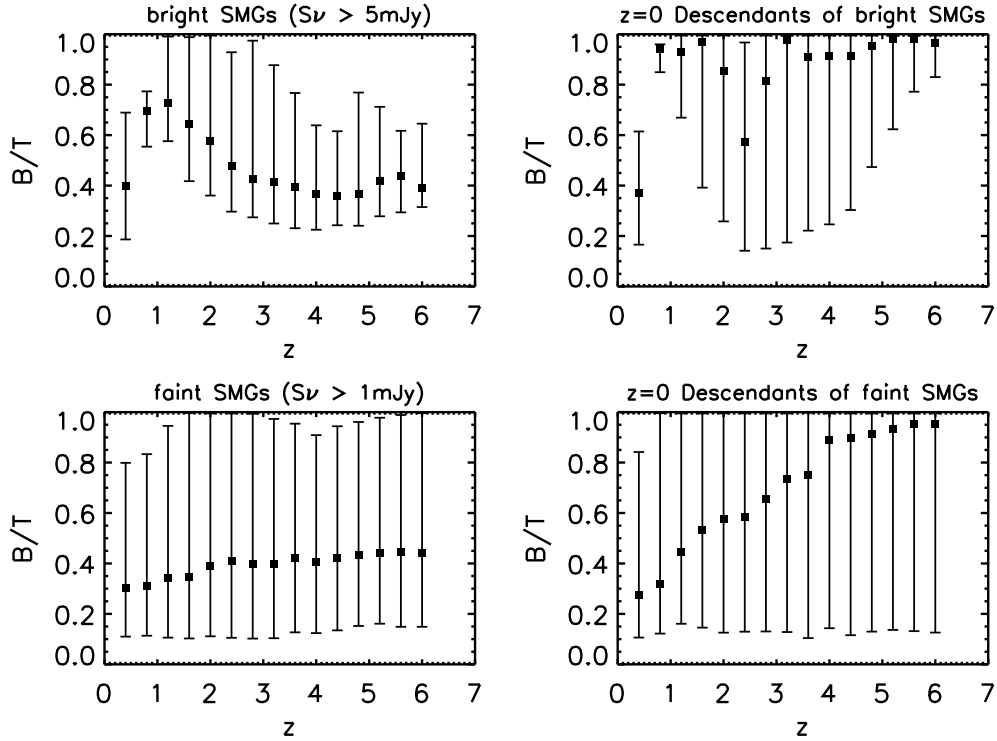


Figure 4. Left panels: The predicted distribution of bulge-to-total stellar mass ratio B/T for SMGs selected at different redshifts. Right panels: the B/T distribution of the $z=0$ descendants of SMGs identified at different redshifts. Top panels: bright SMGs selected with $S_\nu > 5\text{mJy}$. Bottom panels: faint SMGs selected with $S_\nu > 1\text{mJy}$. The filled-squares show the median of the distribution at each redshift and the errorbars indicate the 10% and 90% percentiles. The medians are all calculated for volume-limited samples of SMGs at each redshift.

5.1 Stellar and host halo masses of SMG descendants

What are the masses of the present-day descendants of SMGs seen at different redshifts? In the right panels of Fig. 3, we plot the median stellar and host halo masses of the $z=0$ descendants of the SMGs identified at different redshifts. In these panels, the medians are calculated for a volume-limited sample of SMG progenitors, so that descendants are weighted according to the number of such progenitors. Note that it is possible for a present-day galaxy to have multiple SMG progenitors in different branches of its merger tree (see Fig. 1). We find that bright SMGs at higher redshift typically evolve into somewhat more massive galaxies hosted in more massive haloes compared to bright SMGs found at lower redshifts. The model predicts that galaxies seen as bright SMGs at the median of the observed redshift distribution ($z \sim 2$) increase their stellar mass by one order of magnitude by redshift $z=0$ (from $\sim 2 \times 10^{10} h^{-1} M_\odot$ to $\sim 2 \times 10^{11} h^{-1} M_\odot$).

In Fig. 6 we show the distributions of stellar and halo mass for the $z=0$ descendants of galaxies which had SMG progenitors at $z > 1$. In this figure, and also in Figs. 7 and 8, the distributions are calculated for volume-limited samples of SMG descendants, with each descendant given the same weight whether it had one or more SMG progenitors. The top left panel of Fig. 6 shows the distribution of stellar masses of the descendants of all bright SMGs with $z > 1$. We separate the galaxies into bulge-dominated ($B/T > 0.5$) and disk-dominated ($B/T < 0.5$) samples. The number of bulge-dominated descendants is nearly double the number of disk-dominated descendants. Also, the bulge-dominated descendant galaxies have a higher median mass. For all of the descendants, the median stellar mass is $1.5 \times 10^{11} h^{-1} M_\odot$. The distribu-

tion of host dark matter halo masses of the $z=0$ descendants, plotted in the top right panel of Fig. 6, shows a higher median mass for bulge-dominated than for disk-dominated descendants. The median dark matter halo mass for all $z = 0$ descendants of bright $z > 1$ SMGs is $2.9 \times 10^{13} h^{-1} M_\odot$. For comparison, we also show the results for the faint SMGs selected with $S_\nu > 1\text{mJy}$. The median stellar and dark matter halo masses of the descendants are about 4 times smaller than for the bright SMGs, and the distributions are wider. In this case, the proportions of disk-dominated and bulge-dominated descendants are reversed compared to the bright SMGs, with more than twice as many disk-dominated as bulge-dominated descendants.

In Fig. 7, we repeat the same analysis but separate the descendants into central and satellite galaxies in the halo where they live at the present-day. We can see that nearly 80% of the $z = 0$ descendants of bright SMGs are central galaxies, while this fraction is reduced to 60% for the faint SMGs. We note that satellite galaxies that are descendants of bright SMGs are found only in the more massive haloes today.

We note that Hainline et al. (2010) arrived at a similar estimate to our own for the masses of the present-day descendants of bright SMGs, but starting from observations of SMGs at high redshift, and making different assumptions from ours about their subsequent evolution down to $z = 0$.

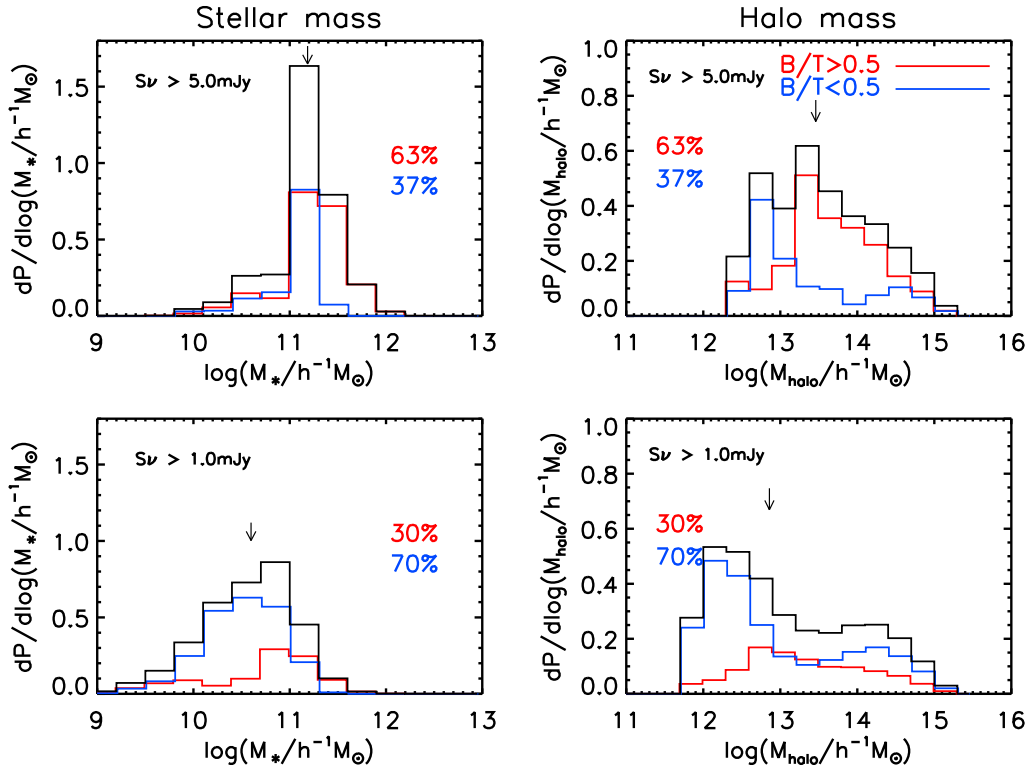


Figure 6. Stellar mass distribution (left panels) and halo mass distribution (right panels) for $z = 0$ descendants of bright $z > 1$ SMGs ($S_\nu > 5 \text{ mJy}$, top panels) and for descendants of faint $z > 1$ SMGs ($S_\nu > 1 \text{ mJy}$, bottom panels). The distributions are for volume-limited samples of descendants, and weight each descendant equally whether it had one or more SMG progenitors. The red distribution is for bulge-dominated ($B/T > 0.5$) descendant galaxies and the blue for disk-dominated ($B/T < 0.5$) descendant galaxies. The black lines represent the sum of the red and blue distributions. The mass distributions are normalized to unit area for the full sample. The vertical black arrows indicate the median of the total distribution in each panel. The percentages in each panel refer to the percentage of bulge-dominated (in red) and disk-dominated (in blue) galaxies.

5.2 Morphology of descendants of SMGs compared to other similar mass galaxies

The top right panel of Fig. 4 shows us that the model predicts that bright SMGs identified at different redshifts typically evolve into highly bulge-dominated galaxies at redshift $z=0$. According to the bottom right panel of Fig. 4, the $z = 0$ descendants of faint SMGs at low and intermediate redshifts have intermediate values of B/T . Only the higher redshift samples evolve predominantly into highly bulge-dominated systems at the present-day.

Fig. 6 shows that the majority of the descendants of bright $z > 1$ SMGs are bulge-dominated systems, while for faint SMGs most descendants are disk-dominated. In Fig. 8 we show (in black) the probability distribution of B/T for the $z = 0$ descendant galaxies of $z > 1$ SMGs (with each descendant given equal weight whether it had one or more SMG progenitors). The top panel shows the descendants of bright SMGs, of which 63% of the descendants are bulge-dominated ($B/T > 0.5$) and 37% are disk-dominated ($B/T < 0.5$). Among these, 42% of the descendants are pure bulge systems ($B/T > 0.9$) and only 6% are pure disk systems ($B/T < 0.1$). The bottom panel of Fig. 8 shows the probability distribution of B/T for the descendants of faint SMGs. In this case, only 30% of the descendants are bulge-dominated systems, with 11% being pure bulge systems, and 12% being pure disk systems.

However, are these results a special characteristic of SMG descendants, or are these morphologies simply typical of $z = 0$ galaxies with similar stellar mass? To answer this, we select com-

parison samples (for bright and faint SMGs) composed of galaxies at $z = 0$ with similar stellar mass distributions to the bright and faint SMG descendants respectively. In Fig. 8, we plot the probability distribution of B/T for the SMG descendants in black, and for the comparison samples in red. The descendant and comparison samples for bright and faint SMGs show very similar distributions. Despite the fact that most of the descendants of bright SMGs are bulge-dominated galaxies, their morphologies are not significantly different from other $z = 0$ galaxies with similar stellar masses.

5.3 Metallicity of descendants of SMGs compared to other galaxies

In the top panel of Fig. 9, we compare the median stellar metallicity (weighted by stellar mass) as a function of stellar mass for galaxies which are descendants of bright SMGs (red curves) to that of other galaxies of the same stellar mass which are not descendants of bright SMGs (blue curves). The medians are calculated for volume-limited samples of present-day galaxies. The dark and light grey shaded regions respectively show the 25-75% and 10-90% ranges for the stellar masses of descendants of bright SMGs. We see that high stellar mass descendants of bright SMGs have very similar metallicities to other present-day galaxies of the same mass, while low stellar mass descendants typically have larger metallicities than high-mass descendants or other galaxies of similar masses. For descendants of the median stellar mass, the median metallicity is only 20% higher than for non-descendants of the same mass, but for the 10% least massive descendants, the difference in median

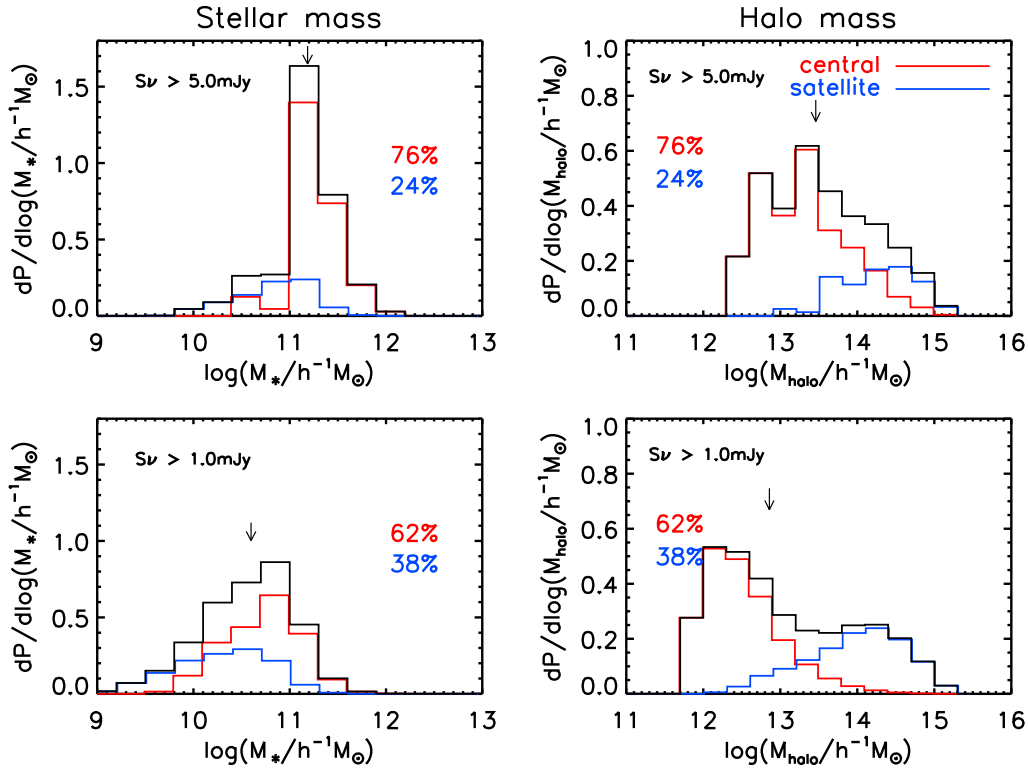


Figure 7. Similar to Fig. 6 but separating the descendant galaxies into central (red) and satellite (blue) galaxies. In this case, the percentages in each panel refer to the percentage of central (upper value) and satellite (lower value) galaxies.

metallicity is a factor 2 or more. It thus appears that for descendants below the median stellar mass, the starburst which powered the SMG was also responsible for chemically enriching the descendant galaxy above the typical level for galaxies of that present-day mass.

The lower two panels of Fig. 9 make similar comparisons of the bulge-to-total stellar mass ratio, B/T , and the halo mass for descendants and non-descendants of bright SMGs. We see that the most massive 90% of descendants have very similar median B/T to non-descendants of the same mass, while the least massive 10% have significantly larger B/T than the non-descendants (up to a factor 2-3). The halo masses for the most massive 75% of descendants are very similar to non-descendants of the same mass, but for the least massive descendants, the median halo masses are much larger (up to a factor $\sim 10^3$).

6 SMG PROGENITORS OF PRESENT-DAY GALAXIES

In the previous section we studied the properties of the descendants of SMGs. We identified SMGs in the model at a particular redshift and we found their $z=0$ descendants. In this section we want to study the connection of SMGs to present day galaxies from the opposite perspective: given a galaxy today with a particular mass, what is the probability that this galaxy had SMG progenitors? And for dark matter haloes at present-day, what is the probability that a progenitor halo hosted at least one SMG? Fig. 10 answers these questions, for the $z = 0$ descendants of both bright and faint SMGs at $z > 1$ (top and bottom panels respectively). The left panels show this probability as a function of stellar mass, and the right panels as a function of halo mass. We see that the probability that a galaxy or halo had one or more SMG progenitors at

$z > 1$ brighter than a given $850\mu\text{m}$ flux increases with increasing mass. From the top left panel, we see that present-day galaxies have a probability of 10% to be descendants of bright SMGs ($S_\nu > 5\text{mJy}$) at a stellar mass of $10^{11}h^{-1}M_\odot$, and 50% at a mass of $6 \times 10^{11}h^{-1}M_\odot$. For comparison, we see from the lower-left panel that 50% of galaxies with present day stellar masses of $2 \times 10^{10}h^{-1}M_\odot$ are descendants of faint SMGs ($S_\nu > 1\text{mJy}$). We find in both cases (bright and faint SMGs) that at intermediate masses ($\sim 10^{10} - 10^{11}h^{-1}M_\odot$) there are more disk-dominated descendants of SMGs than bulge-dominated descendants. For haloes, we see from the right panels that more than 50% of the haloes with masses larger than $10^{14}h^{-1}M_\odot$ are predicted to have bright SMG progenitors, and 50% of the haloes with masses larger than $2 \times 10^{12}h^{-1}M_\odot$ are predicted to have faint SMG progenitors.

7 CONTRIBUTION OF SMGS TO THE PRESENT-DAY STELLAR MASS

We saw in the previous section that most massive galaxies today are predicted to be descendants of SMGs. We found also in Section 4.1 that the median of the SMG phase duration is 0.11 Gyr. Since in the literature a high star formation rate (SFR) is traditionally inferred for the bright SMGs (based on the assumption of a normal IMF), we want to know what contribution to the present-day stellar mass is actually produced in the SMG phase.

In Fig. 11 we plot the predicted evolution of the cosmic SFR density. We show both the total, as well as the contributions from bursts and quiescent disks, and the contributions from galaxies in a bright ($S_\nu > 5\text{mJy}$) or faint ($S_\nu > 1\text{mJy}$) SMG phase. We see that the contribution to star formation from quiescent disks dominates at redshift $z \lesssim 3.5$, but bursts dominate at higher redshifts,

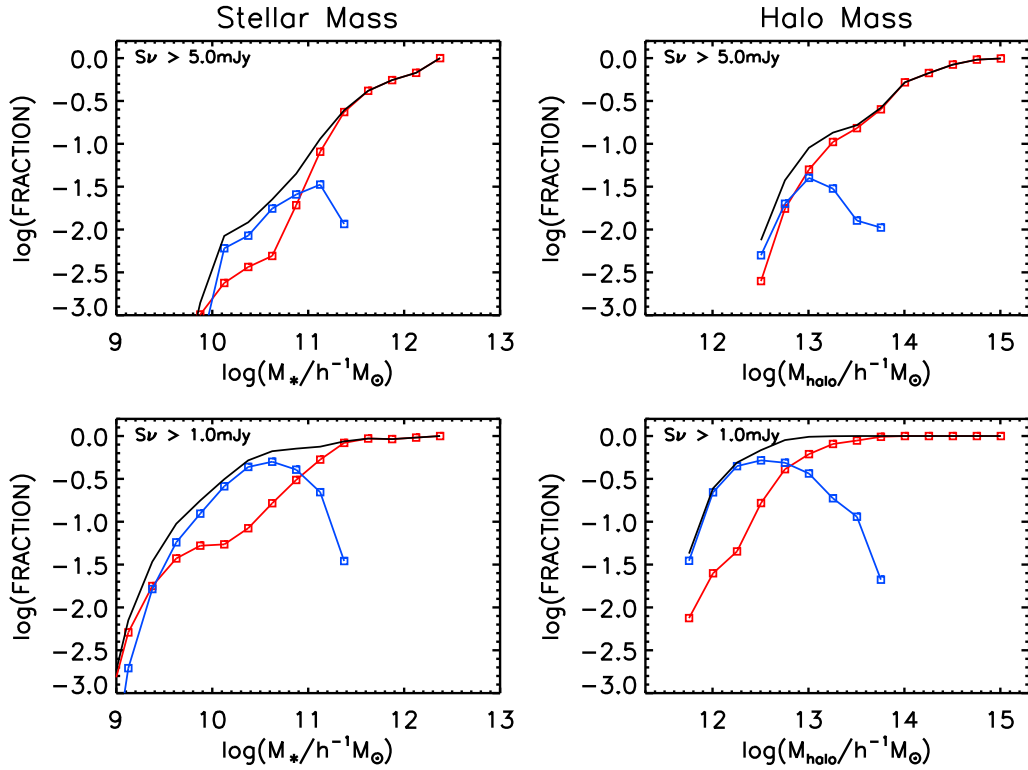


Figure 10. Left panels: fraction of present-day galaxies by stellar mass that are predicted to be descendants of bright SMGs ($S_\nu > 5.0\text{mJy}$, top panel) and descendants of faint SMGs ($S_\nu > 1.0\text{mJy}$, bottom panel). Right panels: fraction of present-day halos by mass that are predicted to have halo progenitors that hosted at least one bright SMG (top panel) or at least one faint SMG (bottom panel). These are computed for $z > 1$ SMG progenitors. Left panels: bulge-dominated ($B/T > 0.5$) descendants in red and disk-dominated ($B/T < 0.5$) descendants in blue. Right panels: bulge-dominated ($B/T > 0.5$) halo central galaxy in red and disk-dominated ($B/T < 0.5$) halo central galaxy in blue. The black line represents all of the SMG descendants (the sum of the blue and red lines).

as found earlier by Baugh et al. (2005). At redshifts $z = 2 - 4$, around 1% of the cosmic star formation is produced by bursts in bright SMGs, and around 10% by bursts in faint SMGs. The quiescent SFR density is typically one order of magnitude smaller than the burst SFR density for bright SMGs at high redshift. For faint SMGs, the burst SFR density dominates at redshift $z \gtrsim 2$, but quiescent star formation becomes more important at lower redshift. At low enough redshift ($z \ll 1$), star formation at any level in a galaxy is sufficient to produce a sub-mm flux above the bright or faint thresholds, which is why the quiescent and burst contributions from bright and faint SMGs converge on the total quiescent and burst contributions at $z = 0$.

In the top panel of Fig. 12 we plot the comoving stellar mass density as a function of redshift, showing both the total, and the contributions to this from star formation in the quiescent and burst modes, and the contributions from star formation during bright and faint SMG phases at $z > 1$. Note that the stellar mass densities we plot are the values after allowing for recycling of gas to the ISM from dying stars, using the recycled fractions for the two IMFs given in Sec. 2.3 (recall that the recycled fraction for the top heavy IMF is close to unity). The lower panel shows the different contributions to the stellar mass density plotted as fractions of the total stellar mass density at that redshift. We see from this that overall, bursts of star formation contribute a total of 5% to the present-day stellar mass density. Star formation (burst+quiescent) in the faint SMG phase at $z > 1$ contributes 2% to the present-day stellar mass density, while the bright SMG phase at $z > 1$ contributes only 0.06%. The contribution of bursts and SMGs to metal production

are however much larger, due to both the larger yield and larger recycled fraction for the burst IMF compared to the quiescent IMF. The model predicts that all bursts over the history of the universe produced 70% of the metals existing today, while bright SMGs at $z > 1$ produced 0.8% of the metals existing today.

Finally, we examine in more detail the contribution of the mass produced by all bursts and by bursts in the bright SMG phase as a function of stellar mass. In Fig. 13 we plot the fraction of the present stellar mass (allowing for recycling) produced by all bursts in all galaxies (red) and only in descendants of bright SMGs (black). We also plot the contribution to the stellar mass produced by bursts and quiescent star formation in the bright SMG phase for all present-day galaxies (green) and only for the descendants of bright SMGs (blue). We see from this plot that on average bursts contribute 3-8% to the present-day stellar masses of galaxies over the whole range $\sim 10^9 - 10^{12} h^{-1} M_\odot$. If we look only at galaxies which are descendants of bright SMGs, then we find an average fraction that is the same at the highest stellar masses, but increases with decreasing mass, reaching 60% for the least massive descendants ($\sim 5 \times 10^9 h^{-1} M_\odot$). However, the total stellar mass produced in the bright SMG phase at $z > 1$ is less than this. For descendants of bright SMGs, the fraction varies from 30-40% for the least massive descendants ($\sim 5 \times 10^9 h^{-1} M_\odot$), to 0.2-0.4% for the most massive ones ($\sim 10^{12} h^{-1} M_\odot$). The average contribution to the current stellar mass of all galaxies from bursts in the bright SMG phase increases with stellar mass, but is always below 0.5%. For a present-day stellar mass of $1.5 \times 10^{11} h^{-1} M_\odot$, which is the median descendant mass of bright SMGs (see Sec. 5.1), the contribution of

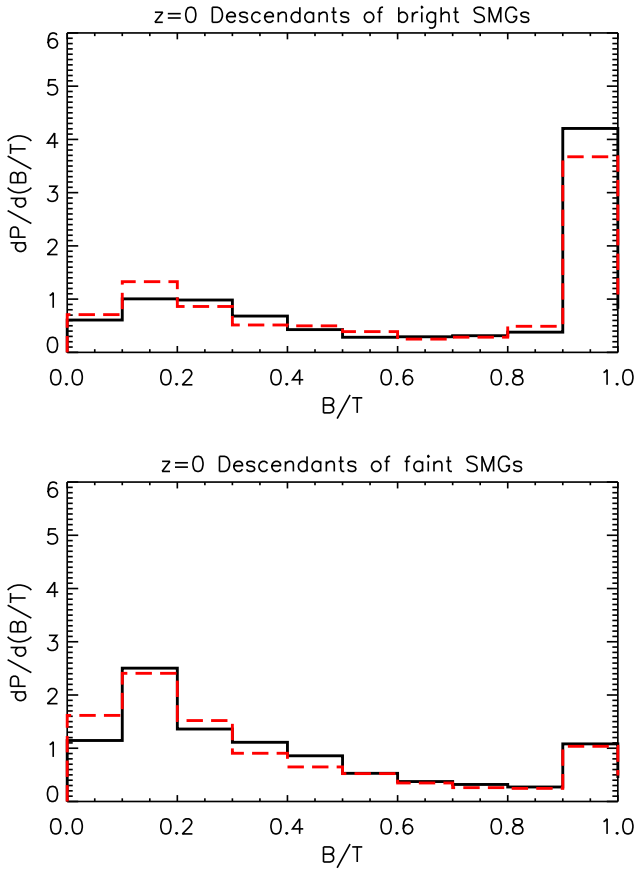


Figure 8. Probability distribution of the bulge-to-total stellar mass ratio (B/T) for $z = 0$ descendants of bright $z > 1$ SMGs (top panel, black) and for descendants of faint $z > 1$ SMGs (bottom panel, black). The distributions are for volume-limited samples of descendants, and give each descendant the same weight whether it had one or more SMG progenitors. The dashed red lines show the B/T distributions of the comparison samples formed by galaxies at $z = 0$ with a similar stellar mass distribution to the bright and faint SMG descendants. All distributions are normalized to unit area under the histogram.

stellar mass produced in the bright SMG phase to the present stellar mass is only 1-2% even for descendants of bright SMGs, and falls to only 0.3% if we look at all galaxies of that mass.

8 CONCLUSIONS

We have investigated predictions for the properties and descendants of submillimetre galaxies (SMGs) in a theoretical model of galaxy formation in a Λ CDM universe (Baugh et al. 2005). This model, which incorporates a top-heavy IMF in starbursts, has previously been shown to reproduce the observed number counts and redshifts of SMGs, as well as a wide variety of other galaxy properties at low and high redshift. We emphasize that Baugh et al. found that the inclusion of a top-heavy IMF in starbursts was essential in order to match both the numbers and redshifts of SMGs and the present-day galaxy luminosity functions in a single model. If instead the IMF was assumed to be universal and of solar neighbourhood form, then by adjusting parameters for feedback and other processes, either the present-day galaxy luminosity functions could be reproduced, but the sub-mm counts underpredicted, or the sub-mm counts could be

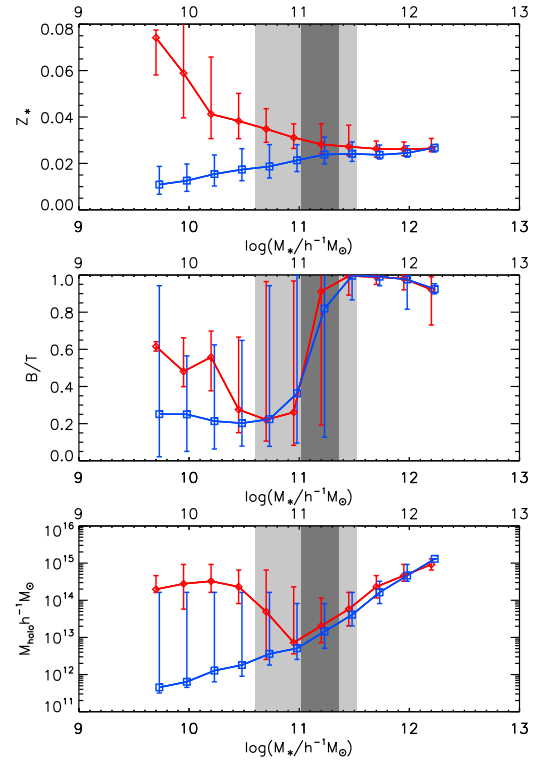


Figure 9. The three panels show the median stellar metallicity, bulge-to-total stellar mass ratio, and halo mass vs. stellar mass for present-day descendants (red line) and non-descendants (blue line) of bright SMGs. The medians are calculated for volume-limited samples of present-day galaxies. The error bars show the 10-90% range in bins of stellar mass. The dark grey shaded region shows the 25-75% range for the stellar masses of descendants of bright SMGs, while the light grey shading shows the 10-90% range.

reproduced, but at the price of predicting far too many high luminosity (and high stellar mass) galaxies at the present day.

We find that bright SMGs in the model, which we define to be objects having $850\mu\text{m}$ fluxes brighter than 5 mJy at some redshift $z > 1$, are typically the progenitors of massive galaxies today, with a median stellar mass $\sim 2 \times 10^{11} h^{-1} M_{\odot}$ for the descendants. The present-day descendants of these bright SMGs are predicted to be mainly bulge-dominated systems, but the bright SMG phase does not appear to play a dominant role in building the bulge, since their morphologies are similar to those of other present-day galaxies with similar stellar masses. The descendants of bright SMGs are also predicted to live in the most massive haloes today. Only the most massive objects in the present-day universe are predicted to be predominantly descendants of bright SMGs – we find that more than 50% of galaxies with masses above $6 \times 10^{11} h^{-1} M_{\odot}$ and halos with masses above $10^{14} h^{-1} M_{\odot}$ have one or more progenitors which hosted bright SMGs at some stage in their evolution.

The model also predicts that the typical stellar masses of bright SMGs at $z = 2$ are $\sim 2 \times 10^{10} h^{-1} M_{\odot}$, similar to the new observational estimates by Hainline et al. (2010), and that they are typically mildly bulge-dominated in stellar mass, consistent with the observations by Swinbank et al. (2010). The typical duration of the bright SMG phase is predicted to be $\sim 0.1\text{Gyr}$, again consistent with observational estimates.

In our model, starbursts account for around 30% of all star formation over the history of the universe. However, stars formed in galaxies which are detectable as bright SMGs at $z > 1$ are pre-

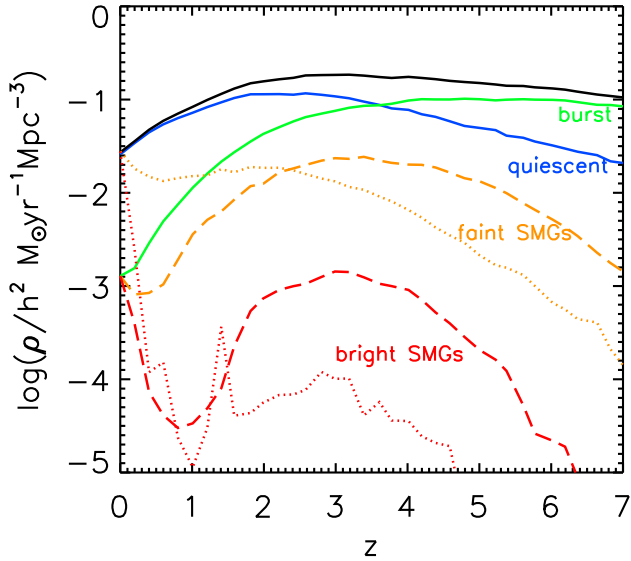


Figure 11. Evolution of the cosmic star formation rate per unit comoving volume. The black line shows the total total star formation rate, while the green and blue lines show the separate contributions from bursts and quiescent star formation respectively. The red and orange lines respectively show the star formation rate in bright and faint SMGs, for which the separate contributions from bursts and quiescent star formation are shown by dashed and dotted lines, respectively.

dicted to account for only 0.06% of the stellar mass density (in live stars and stellar remnants) today. There are two reasons why the latter fraction is so small. Firstly, the recycled fraction for the top-heavy IMF (i.e. the fraction of the initial stellar mass which is returned as gas to the ISM when stars die) is $> 90\%$, much larger than for a solar neighbourhood IMF, so that less than 10% of the stellar mass formed in bursts remains in stars and remnants today. Secondly, only a small fraction of ongoing starbursts at $z > 1$ have high enough star formation rates and luminosities to be detectable as bright SMGs. For present-day galaxies which are descended from bright SMGs at $z > 1$, the fraction of the current stellar mass which was formed in the bright SMG phase is larger, ranging from $\sim 30\%$ in low mass descendants to $\sim 0.3\%$ in the highest mass descendants. However, for median mass descendants, the mean fraction formed in the bright SMG phase is still only $\sim 3\%$.

In summary, our model predicts that SMGs are the progenitors of massive galaxies today. However, most of the stellar mass in these systems is built up by quiescent star formation and then assembled in galaxy mergers, making the contribution of long-lived stars formed during the SMG phase typically very small. The latter is contrary to the view commonly expressed in the observational literature on SMGs. Thus in our model, the SMG phase mainly serves as a “beacon” for gas-rich mergers in the progenitors of massive galaxies at high- z .

ACKNOWLEDGEMENTS

We thank the referee for their constructive report and suggestions which helped to improve the paper. JEG acknowledges receipt of a fellowship funded by the European Commission’s Framework Programme 6, through the Marie Curie Early Stage Training project MEST-CT-2005-021074. This work was supported in part by the

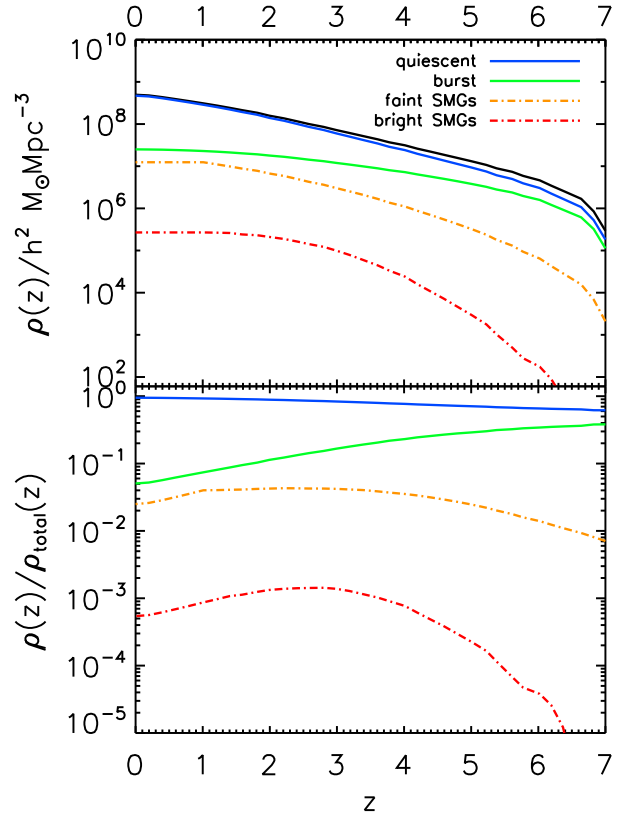


Figure 12. Top panel: comoving stellar mass density as a function of redshift. The black line shows the total, while the blue and green lines show the contributions to this from quiescent and burst star formation respectively, and the red and orange lines show the contributions from star formation in bright or faint SMG phases. For the SMGs, we only show the contributions from SMG phases at $z > 1$. Bottom panel: similar to the top, except that the different contributions to the stellar mass density are plotted as fractions of the total stellar mass density at that redshift.

Science and Technology Facilities Council rolling grant to the ICC. CSF acknowledges a Royal Society Wolfson Research Grant Award.

REFERENCES

- Almeida C., Baugh C. M., Lacey C. G., 2010, ArXiv e-prints (ArXiv:1011.2300)
- Baugh C. M., 2006, Reports on Progress in Physics, 69, 3101
- Baugh C. M., Lacey C. G., Frenk C. S., Granato G. L., Silva L., Bressan A., Benson A. J., Cole S., 2005, MNRAS, 356, 1191
- Benson A. J., Bower R., 2010, ArXiv e-prints
- Benson A. J., Bower R. G., Frenk C. S., Lacey C. G., Baugh C. M., Cole S., 2003, ApJ, 599, 38
- Birnboim Y., Dekel A., 2003, MNRAS, 345, 349
- Bower R. G., Benson A. J., Malbon R., Helly J. C., Frenk C. S., Baugh C. M., Cole S., Lacey C. G., 2006, MNRAS, 370, 645
- Chapman S. C., Blain A. W., Ivison R. J., Smail I. R., 2003, Nature, 422, 695
- Chapman S. C., Blain A. W., Smail I., Ivison R. J., 2005, ApJ, 622, 772
- Chapman S. C., Smail I., Windhorst R., Muxlow T., Ivison R. J., 2004, ApJ, 611, 732

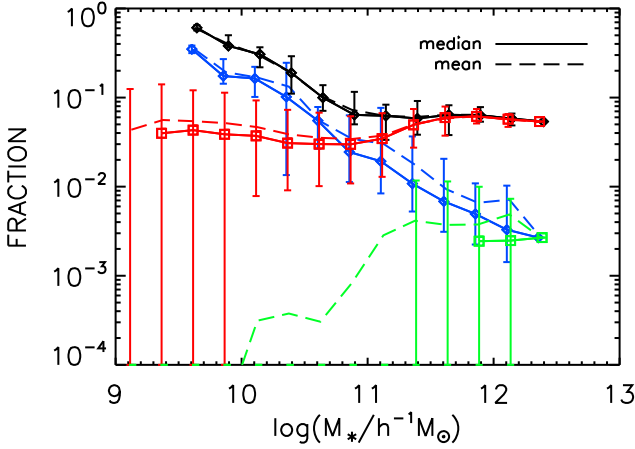


Figure 13. The fraction of the stellar mass produced by different mechanisms as a function of present-day stellar mass. The red lines show the average fraction produced by all bursts in all galaxies, while the black lines show the fraction produced by all bursts in descendants of bright SMGs only. The green lines show the fraction produced by bursts and quiescent star formation in the bright SMG phase for all galaxies, and the blue lines show the fraction produced by bursts and quiescent star formation during an SMG phase in descendants of bright SMGs only. Note that in this plot we only include the contribution of bright SMGs at $z > 1$. The dashed lines show the mean, and the solid lines the median, with the errorbars showing the 10% and 90% percentiles.

Cole S., Lacey C. G., Baugh C. M., Frenk C. S., 2000, *MNRAS*, 319, 168
 Coppin K., Halpern M., Scott D., Borys C., Dunlop J., Dunne L., Ivison R., Wagget al., 2008, *MNRAS*, 384, 1597
 Davé R., Finlator K., Oppenheimer B. D., Fardal M., Katz N., Kereš D., Weinberg D. H., 2010, *MNRAS*, 404, 1355
 Dekel A., Birnboim Y., Engel G., Freundlich J., Goerdt T., Muncuoglu M., Neistein E., Pichon C., Teyssier R., Zinger E., 2009, *Nature*, 457, 451
 Fardal M. A., Katz N., Weinberg D. H., Davé R., 2007, *MNRAS*, 379, 985
 Font A. S., Bower R. G., McCarthy I. G., Benson A. J., Frenk C. S., Helly J. C., Lacey C. G., Baugh C. M., Cole S., 2008, *MNRAS*, 389, 1619
 Fontanot F., Monaco P., Silva L., Grazian A., 2007, *MNRAS*, 382, 903
 González J. E., Lacey C. G., Baugh C. M., Frenk C. S., 2010. In preparation
 González J. E., Lacey C. G., Baugh C. M., Frenk C. S., Benson A. J., 2009, *MNRAS*, 397, 1254
 Granato G. L., Lacey C. G., Silva L., Bressan A., Baugh C. M., Cole S., Frenk C. S., 2000, *ApJ*, 542, 710
 Hainline L. J., Blain A. W., Smail I., Alexander D. M., Armus L., Chapman S. C., Ivison R. J., 2010, *ArXiv e-prints*
 Hughes D. H., Serjeant S., Dunlop J., Rowan-Robinson M., Blain A., Mann R. G., Ivison R., Peacock J., Efsthathiou A., Gear W., Oliver S., Lawrence A., Longair M., Goldschmidt P., Jenness T., 1998, *Nature*, 394, 241
 Kaviani A., Haehnelt M. G., Kauffmann G., 2003, *MNRAS*, 340, 739
 Kennicutt Jr. R. C., 1983, *ApJ*, 272, 54
 Kroupa P., 2001, *MNRAS*, 322, 231
 Lacey C., Cole S., 1993, *MNRAS*, 262, 627
 Lacey C. G., Baugh C. M., Frenk C. S., Almeida C., 2010a. In

preparation

Lacey C. G., Baugh C. M., Frenk C. S., Benson A. J., 2010b, *ArXiv e-prints* (ArXiv:1004.3545)
 Lacey C. G., Baugh C. M., Frenk C. S., Benson A. J., Orsi A., Silva L., Granato G. L., Bressan A., 2010c, *MNRAS*, 443
 Lacey C. G., Baugh C. M., Frenk C. S., Silva L., Granato G. L., Bressan A., 2008, *MNRAS*, 385, 1155
 Michałowski M., Hjorth J., Watson D., 2010, *A&A*, 514, A67+
 Parkinson H., Cole S., Helly J., 2008, *MNRAS*, 383, 557
 Press W. H., Schechter P., 1974, *ApJ*, 187, 425
 Puget J.-L., Abergel A., Bernard J.-P., Boulanger F., Burton W. B., Desert F.-X., Hartmann D., 1996, *A&A*, 308, L5+
 Schurer A., Calura F., Silva L., Pipino A., Granato G. L., Matteucci F., Maiolino R., 2009, *MNRAS*, 394, 2001
 Silva L., Granato G. L., Bressan A., Danese L., 1998, *ApJ*, 509, 103
 Smail I., Chapman S. C., Ivison R. J., Blain A. W., Takata T., Heckman T. M., Dunlop J. S., Sekiguchi K., 2003, *MNRAS*, 342, 1185
 Smail I., Ivison R. J., Blain A. W., 1997, *ApJ*, 490, L5+
 Springel V., White S. D. M., Jenkins A., Frenk C. S., Yoshida N., Gao L., Navarro J., Thacker et al., 2005, *Nature*, 435, 629
 Swinbank A. M., Lacey C. G., Smail I., Baugh C. M., Frenk C. S., Blain A. W., Chapman S. C., Coppin K. E. K., Ivison R. J., González J. E., Hainline L. J., 2008, *MNRAS*, 391, 420
 Swinbank A. M., Smail I., Chapman S. C., Borys C., Alexander D. M., Blain A. W., Conselice C. J., Hainline L. J., Ivison R. J., 2010, *MNRAS*, 405, 234
 Tacconi L. J., Neri R., Chapman S. C., Genzel R., Smail I., Ivison R. J., Bertoldi F., Blain A., Cox P., Greve T., Omont A., 2006, *ApJ*, 640, 228
 van Dokkum P. G., 2008, *ApJ*, 674, 29
 Vega O., Clemens M. S., Bressan A., Granato G. L., Silva L., Panuzzo P., 2008, *A&A*, 484, 631

This paper has been typeset from a \LaTeX file prepared by the author.